

Article

Double-Encapsulated Microcapsules for the Adsorption to Cotton Fabrics

Zuobing Xiao ¹, Wenwen Xu ¹, Jiajia Ma ², Yi Zhao ², Yunwei Niu ¹, Xingran Kou ^{1,2,*} and Qinfei Ke ^{1,2,*}

¹ School of Perfume and Aroma Technology, Shanghai Institute of Technology, Shanghai 201418, China; xzb@sit.edu.cn (Z.X.); 186071225@mail.sit.edu.cn (W.X.); nyw@sit.edu.cn (Y.N.)

² Key Laboratory of Textile Science & Technology, Ministry of Education, College of Textiles, Donghua University, Shanghai 201620, China; 2170043@mail.dhu.edu.cn (J.M.); zhaoyi@dhu.edu.cn (Y.Z.)

* Correspondence: kouxr@sit.edu.cn (X.K.); kqf@sit.edu.cn (Q.K.)

Abstract: Double-encapsulated microcapsules (DEMs) were prepared and effectively adsorbed onto the cotton fabric surfaces during impregnation without crosslinking agents to obtain functional cotton fabrics. Specifically, Fourier transform infrared spectrometer (FTIR) and confocal laser scanning microscope (CLSM) showed two different molecules (lavender essence and dye indigo) were encapsulated into the microcapsules simultaneously, with loading capacity of 10% and 9.73%, respectively. The spherical shape of DEMs was confirmed by transmission electron microscopy (TEM), confocal laser scanning microscope (CLSM) and average particle sizes were about 617 nm, as measured by dynamic light scattering (DLS). According to the results of IR and X-ray photoelectron spectroscopy (XPS) experiments, DEMs was combined with cotton fabrics by hydrogen bond. The superior thermal stability of microcapsules and functional cotton fabrics was also demonstrated. The adsorption behavior and mechanism of microparticles onto cotton fabrics were further examined by chemical property characterization in combination with adsorption kinetic model. The kinetic adsorption process included three stages: fast adsorption, slow adsorption rate, and adsorption equilibrium. Finally, the good color fastness of the functional cotton fabrics was demonstrated by the tests of rubbing and accelerated laundering. Herein, this study will be beneficial to the development of functional cotton fabrics-based materials.

Keywords: microcapsules; supramolecular system; functional cotton fabrics; kinetic adsorption



Citation: Xiao, Z.; Xu, W.; Ma, J.; Zhao, Y.; Niu, Y.; Kou, X.; Ke, Q. Double-Encapsulated Microcapsules for the Adsorption to Cotton Fabrics. *Coatings* **2021**, *11*, 426. <https://doi.org/10.3390/coatings11040426>

Academic Editor: Artur P. Terzyk

Received: 19 February 2021

Accepted: 2 April 2021

Published: 7 April 2021

Publisher's Note: MDPI stays neutral with regard to jurisdictional claims in published maps and institutional affiliations.



Copyright: © 2021 by the authors. Licensee MDPI, Basel, Switzerland. This article is an open access article distributed under the terms and conditions of the Creative Commons Attribution (CC BY) license (<https://creativecommons.org/licenses/by/4.0/>).

1. Introduction

At present, it is necessary to give textiles more new values and functions, such as aesthetics, fragrance, and health care, on the basis of satisfying people's warmth. Color sustenance of human aesthetic taste; hence, the emergence of modern dye to meet people's pursuit of clothing color. Indigo pigment, as one of the most important vat dyes, has excellent water resistance, light resistance, and friction resistance, which is widely used in food, medicine, and in the printing and dyeing industries [1], but its strong low water solubility drastically limits its applications. In addition, the application of essence in perfuming products has become increasingly widespread. Among them, lavender essence not only has a variety of pharmacological and biological activities, but also helps to promote blood circulation and improve the body's immunity and vitality [2–4]. However, for its hydrophobicity, high volatility, and poor stability to light, heat, and moisture, new technical approaches are required to overcome the current limitations of lavender essence. In recent years, microencapsulation technology has been widely used in food [5,6], dyeing and finishing [7,8], coating [9,10] and biotechnology [11], and many other fields, which can effectively improve the physical properties of substances (e.g., dye and essence), improve stability, etc.

It is generally known that cyclodextrins (CDs) are cyclic oligosaccharides composed of α -1, 4-coupled D-glucose units, which can be safely degraded by α -amylase and have

excellent bio-compatibility [12,13]. CDs have a hydrophilic external surface and a relatively hydrophobic inner cavity, which enables them to form inclusion complexes with surfactants that have a hydrophobic moiety by encapsulation of the surfactants within the CD cavities. Thus, CDs are widely used in the construction and tuning of assemblies [14–16]. For instance, a wide variety of surfactants, including ionic surfactants [17,18], zwitterion surfactants [19], nonionic surfactants [20], gemini surfactant [21,22], and mixed surfactants [23–25], among others, can lead to the formation of CD-surfactant inclusion complexes driven by host–guest interactions. These inclusion complexes can then be further assembled into various higher-ordered structures (lamellae, vesicles, nanotubes, fiber, etc.) through hydrogen bonding among the CDs. The numerous benefits provided by the use of vesicles, including their ability to host several compounds with different physicochemical properties, and the presence of an aqueous core and the bilayer, render them of particular interest [26–28]. Vesicles have high versatility in this system, where nano- and micro-sized vesicles become microcapsules that simultaneously encapsulate multiple substances. According to Huang et al. [23], the self-assembly vesicles formed from β -CD and mixed cationic/anionic surfactant inclusion complex have been prepared; nevertheless, the application of molecules-loaded vesicles have not been studied systematically. Moreover, it was found that epichlorohydrin modified β -cyclodextrin had better water solubility as compared with ordinary β -CD. In our previous study [29], epichlorohydrin modified β -cyclodextrin has been used as the wall material to prepare microcapsules for cotton fabrics, however, it had not been used to simultaneously encapsulate multiple substances. Due to the large surface energy and small-scale effect, microcapsules can form a strong adhesion with fibers [30,31], which has been widely used in textile finishing. In addition, it is shown that the potential electrostatic interaction [29,32] and intermolecular hydrogen bonding [33,34] between the microcapsules and the fibers. However, most of the studies focused on the properties and applications of modified fibers, or the combination of microcapsules and fibers with cross-linking agents in the studies, while the mechanism of the adsorption process under mild conditions (such as without cross-linking agents) remains unclear. Therefore, our study hopes to further understand the interaction mechanism between microcapsule and fiber by clarifying the interaction types and adsorption kinetics of microcapsules and cotton fabrics binding without cross-linking agent.

In this work, microcapsules with epichlorohydrin modified β -cyclodextrin as wall material encapsulating two substances simultaneously were applied to cotton fabrics. By microencapsulation, the application limitations of natural dye indigo and essence were solved. The interaction of double-encapsulated microcapsules (DEMs) with cotton fabrics and the adsorption behavior and mechanism were examined by physical and chemical property characterization in combination with adsorption kinetic model. Finally, color fastness properties of cotton fabrics treated by DEMs were investigated. Therefore, we expect that this study will be beneficial to the development of functional cotton fabrics-based materials.

2. Materials and Methods

2.1. Materials

One hundred percent cotton woven fabrics were used in all experiments, which were purchased from Shaoxing Manheng Textile Co., Ltd. (Shaoxing, China). Sodium dodecyl sulfate (SDS, 99%), N,N,N-trimethyl-1-dodecanaminium bromide (DTAB, 99%) and sodium carbonate (Na_2CO_3 , 99%) were purchased from Adamas Reagent, Ltd. (Shanghai, China) and used as received. Epichlorohydrin modified β -cyclodextrin was purchased from Zhiyuan Biological Technology Co., Ltd. (Shandong, China). Indigo (99%) was purchased from Acros Reagent, Ltd. (Shanghai, China). The lavender essence was developed and blended in our laboratory and the aromatic substances and percentage content contained were shown in Table S1. N,N-dimethylformamide (DMF) was purchased from Shanghai Titan Technology Co., Ltd. All other reagents and chemicals were of analytical reagent grade. Ultrapure water was used throughout the study.

2.2. Sample Preparation

A mixed surfactant solution containing SDS and DTAB (the molar ratio was 3:1, $C_{\text{total}} = 10$ mM) was prepared in a glass vial. Subsequently, a 16 mmol/L solution of epichlorohydrin modified β -cyclodextrin was added into the mixed SDS/DTAB surfactant system gradually in the host: guest ratio of 2:1, and a slightly blue color was observed when the mixtures were stirred well to ensure homogeneity and the complete dissolution of epichlorohydrin modified β -cyclodextrin. The resulting mixture was placed in a thermostat at 25 °C for 24 h to reach equilibrium.

Encapsulation experiments were prepared as follows: 16.7 μ L lavender essence and 16.7 mg dye indigo powder were successively injected into 15 mL blank microcapsule solution and then treated with a sonication for 20 min. The unloading indigo was removed by dialysis method.

2.3. Pretreatment of Cotton Fabrics

Cotton fabrics were boiled in a certain concentration of sodium carbonate (Na_2CO_3) solution for 2 h to remove the impurities attached to the fiber surface. Then, the fabrics were cleaned with plenty of deionized water and dried at room temperature. After drying, the fabrics were cut into a size of 2×2 cm².

2.4. Preparation of Functional Cotton Fabrics

The cut cotton fabrics were immersed in the 15 mL of DEMs solution (the pH value of the solution is controlled at 6.4 ± 0.3). The adsorption was performed on a Shaker (ZWF-334, Hangzhou, China) with shaking at 150 rpm for 540 min to get the process of adhesion-free crosslinking agent. The treated cotton fabrics were freeze-dried using a Vacuum Freeze Drier at -55 °C (FD-1A-50, Shanghai, China) for 24 h before the next treatment. Three replicates were performed on all samples.

2.5. Characterization

2.5.1. Dynamic Light Scattering (DLS) Measurements

DLS measurements were conducted on a NanoBrook Omni light scattering apparatus (Brookhaven, GA, USA), equipped with a 35 mW optically pumped semiconductor laser. The scattering angle was fixed at 90°.

2.5.2. Transmission Electron Microscopy (TEM) Observations

The morphologies of the DEMs were observed using a Tecnai G2 20 TWIN (FEI, Hillsboro, The Netherlands) transmission electron microscope. For a negatively stained specimen, a drop of sample was placed on 230-mesh copper grid coated with Formvar film. Excess water was removed with filter paper, followed by negative staining of the film with a phosphotungstic acid solution (0.2%). After removal of the excess staining liquid using filter paper, the samples were allowed to dry at room temperature (25 °C) prior to TEM observations.

2.5.3. Fourier Transform Infrared Spectroscopy (FT-IR) Observations

FT-IR measurements were performed on a Nicolet iN10 spectrometer (Thermo Fisher Scientific, Waltham, MA, USA). The samples were mixed with KBr to form transparent sheets prior to carrying out the FT-IR measurements. DEMs-cotton fabrics were directly detected after freeze-drying for 24 h.

2.5.4. Confocal Laser Scanning Microscope (CLSM) Observations

Morphological analysis was performed using skyscan1276 CLSM (Brookhaven, NY, USA). The lavender essence of the DEMs was labeled with Nile red, while the dye Indigo emitted fluorescence under excitation of 405 nm light. An aliquot (50 μ L) of the stained DEMs was dropped onto a glass slide, a cover slip was placed over the solution, and the sample was observed by CLSM using lasers operating at 405 and 488 nm.

2.5.5. Scanning Electron Microscopy (SEM) Observations

Morphological analysis was studied using Gemini 300 SEM (Zeiss, Tokyo, Japan). Prior to investigate morphologies and microstructures, the samples were coated with a thin layer of gold.

2.5.6. Determination of the Loading Capacity

The amount of original and unloading indigo was analyzed by UV-VIS (U-3900, Hitachi, Tokyo, Japan) at a wavelength of 611 nm. The indigo loading capacity (LC) was calculated using the following formula.

$$LC(\%) = \frac{M_t - M_u}{M_{\text{DEMs}}} \times 100\% \quad (1)$$

where M_t was the total weight of indigo added, M_u was the unloaded weight of indigo, and M_{DEMs} was the total weight of DEMs.

2.5.7. Thermo-Gravimetric (TG) Analyses

The thermal properties of the samples were evaluated using a Q5000 thermal analyzer (TA Instruments, New Castle, DE, USA). 4 mg powdered samples after freeze-drying were heated from 30 °C to 600 °C at 10 °C/min under the constant flow of nitrogen by TGA measurement.

2.5.8. X-ray Photoelectron Spectroscopy (XPS)

To characterize the surface chemical differences of the cotton fabrics before and after DEMs adsorption, XPS was applied through K-Alpha photoelectron spectrometer (Thermo Scientific, Waltham, MA, USA). The photoelectron spectrometer was set to 6 mA, 12 kV, and 100 W, respectively, and the photon energy was set to 1486.6 eV. The high-resolution scan of the C1s area took the pass energy at 80 eV. These values of binding energy at 284.8 eV, which were responding to C1s photoelectron emission signals.

2.5.9. Statistical Analysis

All data experiments were performed at least three times and the bars in graphs are presented as mean \pm SD. Variance analysis was conducted using SPSS 21.0 software (SPSS Inc., Chicago, IL, USA), and multiple comparisons were conducted at a 5% significant level ($p < 0.05$).

2.6. Adsorption and Kinetics Study

The concentration of DEMs in the aqueous solutions was determined by U-3900 UV-spectroscopy (Hitachi, Japan). Since lavender essence is composed of a variety of aroma substances, it is broadened at the wavelength of 200–300 nm (Figure S1a). Therefore, the maximum absorption wavelength of lavender essence is not easy to obtain directly. At present, it is mainly obtained by testing its main components in some studies [35–37]. Hence, the dye indigo was used as a marker to select the detection wavelength. The results showed that the maximum absorption wavelength of indigo standard solution at 611 nm (Figure S1b), which was consistent with the literature [38]. Therefore, the freeze-dried functional cotton fabrics were placed in a glass bottle, and 15 mL of DMF as an extractant was added to it, and shaken in a shaker (ZWF-334, Shanghai Zhicheng Analytical Instrument Manufacturing Co., Ltd., Shanghai, China) at 150 rpm for 12 h (The temperature is maintained at 25 °C), and then scan at 611 nm with an ultraviolet spectrophotometer to measure the absorbance to obtain the amounts of adsorbed particles on the cotton fabrics. For quantification of microparticles, peak areas were compared to a calibration curve ($y = 0.0524 + 0.5312x$, $R^2 = 0.999$) by indigo standard solutions (Figure S2).

At 25 °C, functional fabrics were prepared by the above method (see Section 2.4) for immersion time of 5, 10, 15, 20, 25, 30, 35, 40, 45, 50, 60, 120, 180, 300, 420, and 600 min,

respectively. UV spectrophotometric measurements were performed, the amount of DEMs adsorbed at time t , Q_t (mg/g) was calculated with the following equation (Equation (2)):

$$Q_t = \frac{CV}{W} \quad (2)$$

where C (mg/L) represent the DEMs concentrations at time t , V (L) represent the volume of the solution and W (g) represent the cotton fabrics weight. The experiment was performed in triplicate. Furthermore, the pseudo-first-order kinetic model (Equation (3)), pseudo-second-order kinetic model (Equation (4)) and Bangham kinetic model (Equation (5)) were used to fit the experimental data to evaluate the performance of the adsorption for DEMs onto cotton fabrics. Weber Morris interparticle diffusion model (Equation (6)) was used to further describe the mechanism of the adsorption process.

$$\ln(Q_e - Q_t) = \ln Q_e - k_1 t \quad (3)$$

$$\frac{t}{Q_t} = \frac{1}{k_2 Q_e^2} + \frac{1}{Q_e} \quad (4)$$

$$Q_t = Q_e \left(1 - e^{-k_b t^z}\right) \quad (5)$$

$$Q_t = k_i t^{\frac{1}{2}} + C \quad (6)$$

where Q_t (mg g⁻¹) was the amount of DEMs adsorbed at different times intervals t (min) and Q_e (mg g⁻¹) was the equilibrium adsorbed amount of DEMs; k_1 (min⁻¹), k_2 (g mg⁻¹ min⁻¹), k_b (min⁻¹), and k_i (mg g⁻¹ min^{-0.5}) were the rate constants of the pseudo-first-order, pseudo-second-order, Bangham and Weber Morris interparticle diffusion model, respectively. Where z was a constant in Bangham kinetic model and C was boundary layer thickness (mg/g) in Weber Morris interparticle diffusion model.

2.7. Tests for Color Fastness to Rubbing

According to Chinese national standard (GB/T 3920-2008) "Textiles-Tests for color fastness-Color fastness to rubbing", the color fastness to rubbing (dry rubbing) of functional cotton fabrics was determined by a friction tester (SHK-T104, Shanghai Hengke Instrument Technology Co., Ltd., Shanghai, China). Samples were rubbed for 10 times at the friction rate of 1 time/second after tiled and fixed. The color fastness level was evaluated with the gray sample card.

2.8. Tests for Accelerated Laundering

The color fastness to washing of functional cotton fabrics was performed by a laundering machine (SHK-T133, Shanghai Hengke Instrument Technology Co., Ltd., Shanghai, China) according to AATCC 61-2013 "Colorfastness to Laundering, Home and Commercial: Accelerated". Sample were washed at 40 °C for 45 min. The washed fabrics were ultrasonicated in water and dried prior to further characterization. Similarly, the color fastness level was evaluated with the gray sample card.

All data experiments were performed at least three times.

3. Results and Discussion

3.1. Characterization of DEMs

Subsequently, the encapsulation of such different substances, namely dye indigo and lavender essence, was investigated using the vesicles, leading to form DEMs. There were no floating oil beads on the surface of the DEMs and it can be considered that lavender essence was completely encapsulated, that is, the loading amount is 10%. According to determination of the loading capacity by UV-VIS, there was a high-loading content of indigo, up to 9.73%. Figure 1a showed that Dynamic light scattering (DLS) result of the average size of the DEMs was about 617 nm with a narrow size distribution. Transmission

electron microscopy (TEM) images suggested that uniform and evenly distributed spherical morphology with distinct color contrast between the center and the shell of the components, indicating the formation of vesicular structure after the simultaneous encapsulating of indigo and lavender essence, as well (Figure 1b), the experimental results are consistent with literature [26]. Due to the ability of indigo dye to fluoresce, CLSM was performed, and the obtained results were consistent with TEM observations (Figure 1c). To confirm whether the different species were encapsulated into the microcapsules, IR spectra were carried out. The IR spectra of blank microcapsules, DEMs, lavender essence and indigo were obtained. As shown in Figure 1d, the wide characteristic absorption band of blank microcapsules was observed at 3446 cm^{-1} , corresponding to the association of OH groups. The remaining peaks represented stretching of methyl group (2923 cm^{-1}) and methylene group (2851 cm^{-1}). The characteristic peaks of DEMs were similar to blank microcapsules, indicating that blank microcapsules were the main body. Nevertheless, the OH vibration of DEMs moves slightly to the higher wavenumber (3466 cm^{-1}) than the blank microcapsules. This was for the reason that the capsulated essence was mostly terpenoids, which were prone to form hydrogen bonds. In the spectrum of lavender essence, a characteristic peak was observed at 3466 cm^{-1} , which may be attributed to the expansion and contraction of the hydrogen bond O–H. The peak of C=O at 1740 cm^{-1} and CO- at 1250 cm^{-1} was due to the stretching of ester groups from linalool or linalyl acetate groups [39]. In the spectrum of indigo, a characteristic peak was observed at 3269 and 3040 cm^{-1} , which were attributed to the stretching vibration of the N–H and the joint stretching vibration of C=O and intramolecular hydrogen bond, respectively. Additional sharp characteristic absorption peak was observed at 1629 cm^{-1} , which was due to the stretching vibration of the C=C conjugate system, which was also the characteristic absorption peak of indigo molecules [40,41]. To further confirm that the lavender essence and indigo were capsulated in the microcapsules, the enlarged partial IR spectrum was shown (Figure 1e). In the spectrum of indigo, the typical absorption bands at 1484 cm^{-1} and 1462 cm^{-1} for the stretching vibration of C–C in five-membered ring, and the peaks of =C–H at 1315 cm^{-1} , 1298 cm^{-1} and 1071 cm^{-1} were due to the in-plane bending of CH on the aromatic ring. Slight peaks mentioned above were observed in the DEMs, indicating that indigo was encapsulated by the particles. In the spectrum of lavender essence, the peaks at 1170 cm^{-1} for the stretching vibration of C–C of ester groups from linalool or linalyl acetate groups, which was observed in the DEMs, indicating that lavender essence was encapsulated by the particles. CLSM showed the lavender essence and indigo had been well encapsulated into the microcapsules intuitively. Since indigo dye can fluoresce at 300 nm and its fluorescence peak is located at 405 nm, merely the hydrophobic lavender essence was stained (i.e., using Nile Red). It should be noted that only the materials at the micrometer level can be observed by CLSM. For better observation, we selected microcapsules with larger particle sizes in the field of view for observation. As shown in Figure 1f–h, the obtained particles were spherical, with a blue fluorescence core (the indigo phase) and a red fluorescence shell (the Nile Red-stained essence phase). To observe the microstructures of the DEMs in more detail, an indigo dye stain (Figure 1g) and a Nile Red-stained lavender essence stain (Figure 1h) were observed separately. These images confirmed that the microcapsules consisted of an indigo dye core surrounded by a Nile Red-stained lavender essence shell. According to the above experimental results, it was proved that lavender essence and dye indigo were successfully encapsulated in the microcapsules for this system.

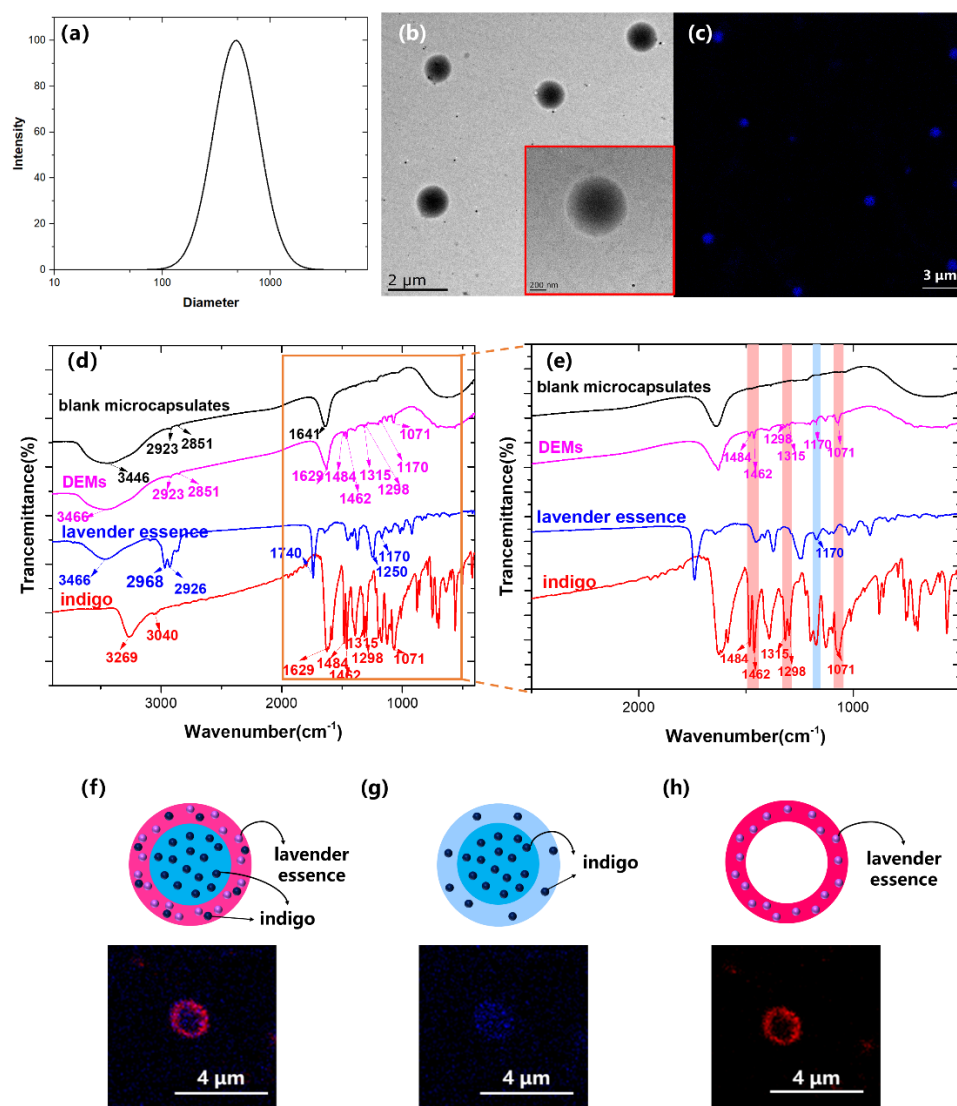


Figure 1. (a) Dynamic Light Scattering (DLS) results, (b) Transmission Electron Microscopy (TEM) images and (c) Confocal Laser Scanning Microscope (CLSM) image of DEMs. (d) Fourier Transform Infrared Spectroscopy (FT-IR) spectra and (e) enlarged partial IR spectra of blank microcapsules, DEMs, lavender essence and indigo. (f–h) Schematic representations and CLSM images of the microcapsules containing both molecules, indigo dye, and the Nile Red-stained lavender essence.

3.2. Adsorption of DEMs on Cotton Fabrics

As shown in Figure 2a, the functional cotton fabrics were successfully prepared by immersing the pre-treated cotton fabrics in the DEMs solution, which transformed from white to blue, with a pleasant lavender fragrance. SEM tests were performed on untreated cotton fabrics, DEMs and cotton fabrics that were combined with DEMs to observe the surface morphology. It can be seen that the surface of the fibers of untreated cotton fabrics was clean and smooth, which was no particle attachment (Figure 2c,d). However, the surface of fibers treated with microcapsules was obviously covered with a number of particles (Figure 2e). It can be clearly observed that the surface of the cotton fabrics (Figure 2f) was attached to spherical particles, whose morphology was consistent with DEMs (Figure 2b) at 100 k times magnification. In the SEM image, the particle size of microcapsules became larger, which may be caused by particle agglomeration in the course of drying. The above results indicated that DEMs could adhere to the surface of fibers. At the same time, the morphology of some DEMs attached to the surface of the fiber changed

from spherical to flake, which may be due to the certain interaction between the fiber and DEMs during combining.

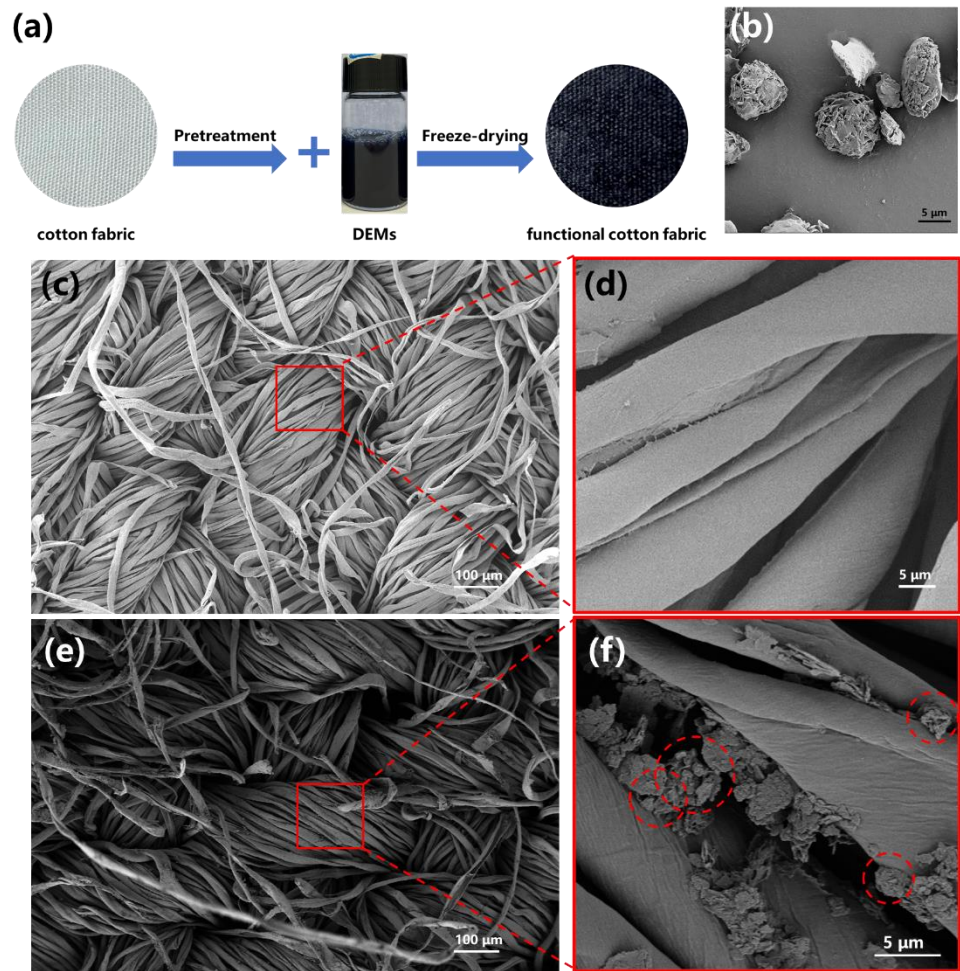


Figure 2. (a) Schematic diagram of the preparation of functional cotton fabrics; Scanning Electron Microscopy (SEM) images of (b) DEMs, (c) untreated cotton fabrics and (e) DEMs-cotton fabrics; Enlarged partial SEM images of (d) untreated cotton fabrics and (f) DEMs-cotton fabrics.

The changes of the surface chemical structure were analyzed by FT-IR. As shown in Figure 3a, the characteristic absorption band of untreated cotton fabrics and DEMs-cotton fabrics was observed at 3341 cm^{-1} , corresponding to the stretching vibration of OH groups. Additionally, the absorption peak of OH groups of DEMs-cotton fabrics became wide and the peak strength decreased compared with blank cotton fabrics, indicating that the hydrogen bond was formed after DEMs absorption. In the enlarged partial IR spectra (Figure 3b), the cotton fiber exhibited the stretching vibration of the C=C conjugate system at 1629 cm^{-1} and the stretching vibration of C-C in five-membered ring at 1484 cm^{-1} and 1462 cm^{-1} after DEM processing, which were present in DEMs. It further indicated that DEMs could adhere to the surface of cotton fibers.

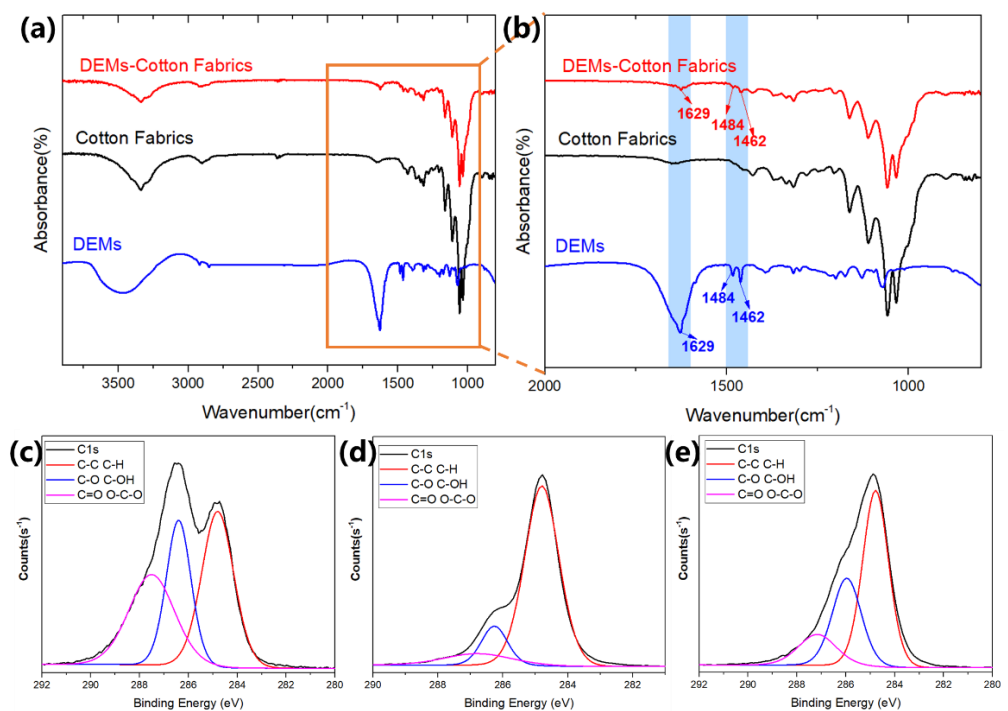


Figure 3. (a) IR spectra and (b) enlarged partial IR spectra of DEMs-cotton fabrics, cotton fabrics and DEMs. High-resolution X-ray Photoelectron Spectroscopy (XPS) spectra for C1s peaks of (c) cotton fabrics (d) DEMs, and (e) DEMs-cotton fabrics.

The interaction between DEMs and cotton fabrics was further studied by analyzing the changes of surface chemical composition of DEMs, cotton fabric and DEMs-cotton fabrics through XPS. As shown in Figure 3c–e, the C1s spectra were divided into three peaks of different intensities. Specifically, peak C1 was assigned to C–C or C–H bonds, peak C2 represented C–O bonds, and peak 3 pointed to C=O, O–C–O, respectively. Table 1 showed relative area, and ratio of cotton fabrics before and after microcapsule adsorption. With the absorption for DEMs onto cotton fabrics, the relative areas of C1, C2, and C3 peak changed dramatically. Obviously, the peak area of C2/C3 was progressively increased to generate higher ratio of C2/(C1 + C3) in contrast to pure cotton fabrics. Since the C2 peak was attributed to the acidity of the fiber, and the C1 and C3 peaks were related to the alkalinity of the fiber, the acidity of the cotton fabrics was enhanced by the adsorption of the DEMs. This finding was consistent with the study of Wang et al. [42]. It further proved the hydrogen bonding interaction between DEMs and cotton fabrics.

Table 1. C1s deconvolution XPS data of cotton fabrics and DEMs-cotton fabrics of the relative peak areas of C groups.

| Samples | Relative Peak Areas (%) | | | Ratios |
|---------------------|-------------------------|-------|-------|--------------|
| | C1 | C2 | C3 | C2/(C1 + C3) |
| cotton fabrics | 38.58 | 25.94 | 35.49 | 0.3502 |
| DEMs-cotton fabrics | 55.35 | 30.63 | 14.02 | 0.4415 |

The thermal stability of microcapsules and functional cotton fabrics can be determined via TG analysis. Figure 4 shows the TG and derivative thermal gravimetry (DTG) curves of pure cotton fabrics, DEMs-cotton fabrics and DEMs, respectively. There were four different degradation inflection points of DEMs which were considered as the peak values of weight loss curves. The initial phase of weightlessness occurred below 100 °C, corresponding to the water loss. The stage of relatively gentle weight loss that occurred from 100 to

190 °C belonged to the evaporation of lavender essence. The thermal evaporation of lavender essence shifted to a much higher temperature due to lavender essence was encapsulated into the microcapsules successfully [43,44]. A rapid loss of weight was seen between 232 and 310 °C, which was ascribed to the decomposition of wall material, namely, epichlorohydrin modified β -cyclodextrin. Finally, the slight weightlessness in the range of 310–382 °C was due to the decomposition of the indigo encapsulated. These results were consistent with the previous report that microencapsulation could improve the thermal stability of the encapsulated material to a certain extent [43,45]. For cotton fabrics, the weight loss at 305–379 °C was mainly caused by the decomposition of fibers. The two main degradation points were oriented at 281 and 378 °C after DEMs adsorption, respectively. The research findings demonstrated that DEMs were adsorbed on cotton fabrics surfaces. The TG curve also illustrated that DEMs still had mass residues even at 600 °C, which proved that the cyclodextrin had good thermal stability as a cotton fabric material [46].

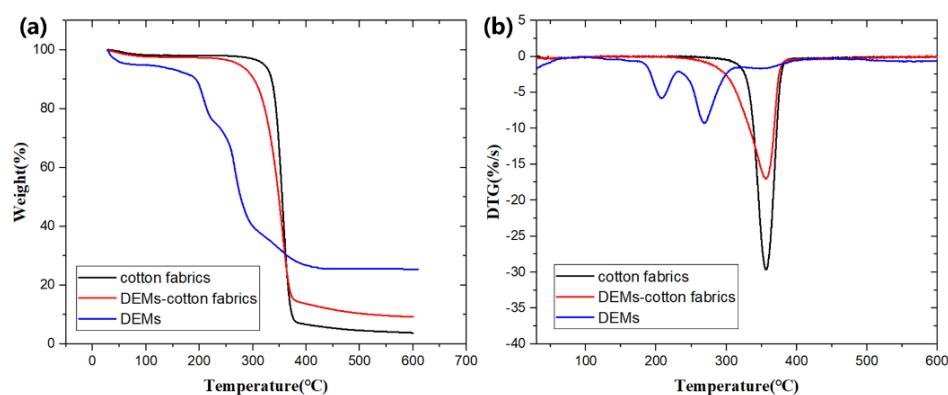


Figure 4. (a) Thermo-gravimetric (TG) curves and (b) Derivative thermal gravimetry (DTG) curves of pure cotton fabrics, and DEMs-cotton fabrics and DEMs.

3.3. Characterization of Adsorption Kinetics

In order to study the migration and binding action of microparticles on the surface of cotton fibers, a kinetic model for the adsorption of DEMs by cotton fabrics was established. The adsorption capacity of DEMs onto cotton fabrics increased with time is shown in Figure 5a. It can be seen that the adsorption process could be divided into two stages, that is to say rapid adsorption within the first 50 min, thereafter, it was slowed down and gradually approached equilibrium. After 9 h, the amount of DEMs absorbed reached to 116.6 mg/g. In previous studies [34,47–49], some scholars had put forward the adsorption theory. They believe that the natural particles reaching equilibrium onto adsorbents in a relatively short time may be driven by intermolecular forces. In the first stage of adsorption, there were adequate binding sites for DEMs on the surface of cotton fabrics, which was the factor for the fast adsorption rate. Subsequently, as the number of binding sites for adsorption and the concentration of microparticles decreased, the adsorption process slowed down to reach equilibrium.

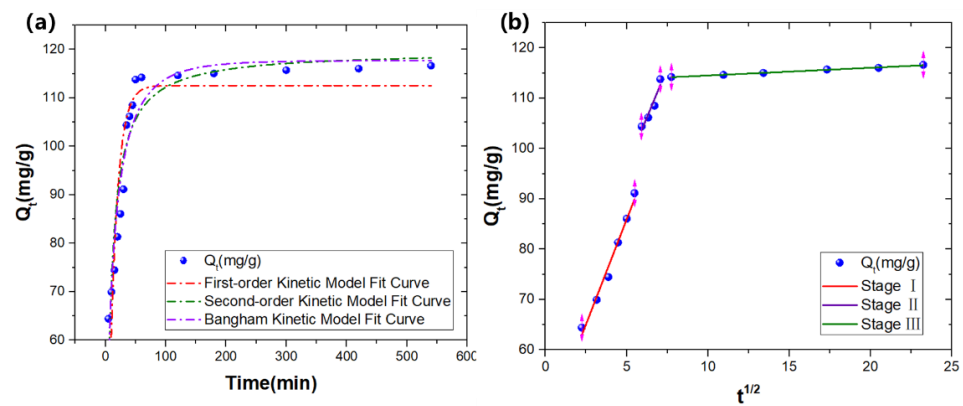


Figure 5. Adsorption of DEMs onto cotton fabrics. Fitting of data to (a) the pseudo-first-order kinetic model, the pseudo-second-order kinetic model, the Bangham kinetic model and (b) the Weber and Morris intraparticle diffusion.

The dynamic adsorption curve was fitted and analyzed by the pseudo-first-order kinetic model, pseudo-second-order kinetic model, Bangham model and intraparticle diffusion model (Figure 5); further, the mechanism of the dynamic migration for microparticles onto the surface of cotton fibers was discussed by combining the fitting coefficients of the related equations. The kinetics parameters and correlation coefficient (R^2) are given in Table 2. Compared to the pseudo-first-order kinetic model, the fitting of the models showed that the $Q_{e,exp}$ of the pseudo-second-order kinetic model was closer to the $Q_{e,cal}$ and the correlation coefficient (R^2) was higher indicating that adsorption was affected by numerous factors [50]. Similar findings have been made regarding the adsorption of polymer particles on the base material (e.g., paper cellulose, cotton fibers, etc.) [34,51,52], showing that the adsorption of DEMs onto cotton fibers may follow a similar mechanism, namely physical adsorption process. However, the pseudo-first-order and pseudo-second-order kinetic models of the adsorption process showed R^2 values were lower than 0.9, while R^2 value of the Bangham model was 0.920. Therefore, the Bangham model fitted better, since it had higher R^2 and lower RE values, suggesting that adsorption of DEMs occurs by diffusion into the pores in the cotton fabric fibers. The Bangham model indicating that it was vital that both the surface and the diffusion of the pore in adsorption [53,54].

Table 2. Kinetic parameters in the DEMs adsorption onto cotton fabrics.

| Pseudo-first-order | | | | |
|-------------------------|--|------------------------------------|-------|--------|
| | K_1 (min^{-1}) | $Q_{e,cal}$ (mg g^{-1}) | R^2 | RE (%) |
| | 0.080 | 112.5 | 0.764 | 3.5 |
| Pseudo-second-order | | | | |
| | K_2 ($\text{g mg}^{-1} \text{min}^{-1}$) | $Q_{e,cal}$ (mg g^{-1}) | R^2 | RE (%) |
| | 0.001 | 119.7 | 0.884 | 2.7 |
| Bangham | | | | |
| | K_b (min^{-1}) | $Q_{e,cal}$ (mg g^{-1}) | R^2 | RE (%) |
| | 0.251 | 117.7 | 0.920 | 0.9 |
| Intraparticle Diffusion | | | | |
| | K_i ($\text{mg g}^{-1} \text{min}^{-0.5}$) | C | R^2 | RE (%) |
| StageI | 8.329 | 44.3 | 0.983 | - |
| StageII | 7.852 | 57.1 | 0.919 | - |
| StageIII | 0.153 | 113.0 | 0.993 | - |

$Q_{e,exp}$: experiment data; $Q_{e,cal}$: calculated form the model. RE (%): the relative error between experimental data (namely 116.6 mg g^{-1}) and calculated data from the model of Q_e .

Weber and Morris used an intraparticle diffusion model to describe the adsorption process, in particular the mass transfer mechanism from the outer surface to pores of the adsorption material [55–58]. Generally, intraparticle diffusion model was used to describe the adsorption process of molecules from a liquid phase onto a solid adsorbent, involving three phases: film surface diffusion, intraparticle diffusion inside, and equilibrium [47,51]. Thereafter, the adsorption process for microparticles onto cotton fabrics was further studied using intraparticle diffusion model. As shown in Figure 5b, the adsorption process was separated into three parts by linear fitting based on this model. This indicated that intraparticle diffusion was not the limiting stage since none of the stages cross the origin. Provided that there was no intraparticle diffusion, the model could account for the predominant mechanism through an individual analysis of the behavior of each stage [53]. For the adsorption of DEMs with cotton fabrics, the calculated turning point was 54 min. In the first stage, the adsorption capacity increased rapidly. After 54 min, the adsorption process slowed down, and reached adsorption saturation in the third stage. The high values of R^2 and K_i indicated that the intraparticle diffusion model fitted well and the adsorption mechanism was dominant. It was suggested that the predominant mechanism was diffusion. The results indicated that the adsorption of microparticles onto cotton fiber surfaces could be separated from three stages: fast adsorption, slow adsorption rate, and adsorption equilibrium. This confirmed that the predominant mechanism was diffusion in the pores, which can be represented: (1) mass transfer or diffusion of DEMs from the solution to cotton fabrics during the rapid adsorption stage; (2) diffusion of DEMs in the voids between cotton fabric fibers in the second stage; and (3) the saturation of all available surface sites of cotton fabrics was achieved at the final stage, similar findings have been reported by several research teams [53,55,58].

3.4. Tests for Color Fastness

The color fastness of functional cotton fabrics, as a kind of daily necessities, is exceedingly important in daily life, including rubbing resistance and washing resistance. According to standards, the friction resistance and washing resistance of functional cotton fabrics were verified by tests for rubbing and accelerated laundering respectively, which were evaluated by contrast color fastness level, microcapsule residual content and SEM observation. By comparing the staining conditions, it was shown that the functional cotton fabrics had excellent friction resistance and potential washing resistance (Table 3). As shown in Figure 6a,b, it was intuitively seen that DEMs still were adsorbed onto the surface of the cotton fabrics after friction according to SEM images, but the particles became smaller and more evenly distributed. Furthermore, the content of DEMs on functional fabrics after friction was 81.4% by UV analysis, which was crucial to improve rubbing performance. In addition, the functional cotton fabrics prepared under mild conditions (without crosslinkers) still retained 21.7% of DEMs under intense washing conditions (washing at 40 °C for 45 min). It was exciting to discover that the remaining DEMs retain their original morphology although the majority of the DEMs fall off during washing (Figure 6c,d), indicating the stable performance of the obtained functional cotton fabrics.

Table 3. Effect of different test methods on color fastness of functional cotton fabrics.

| Serial Number | Test Methods | Color Fastness Level |
|---------------|------------------------|----------------------|
| 1# | Rubbing | 4–5 |
| 2# | Accelerated laundering | 2 |

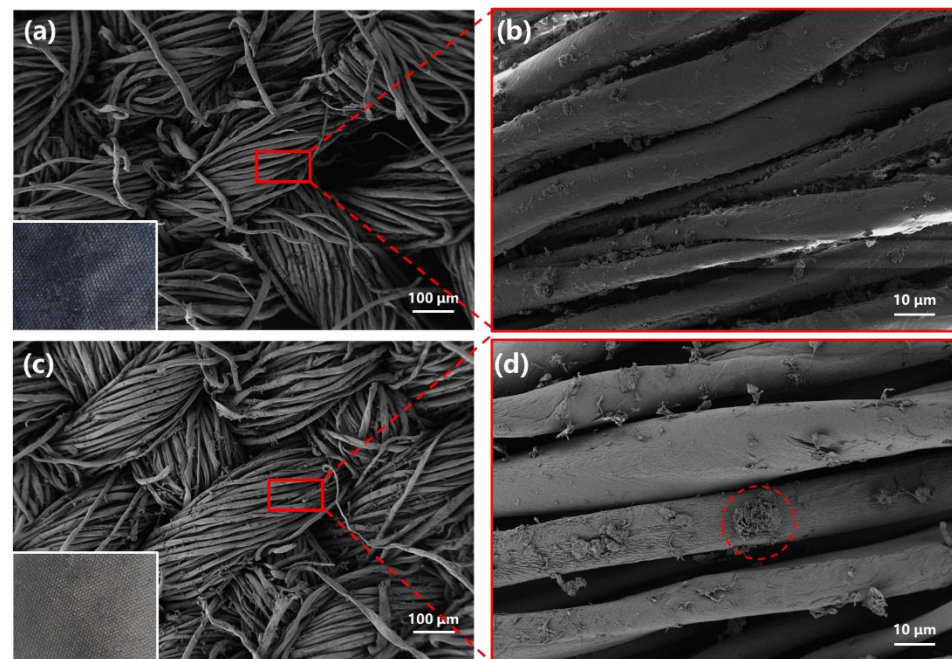


Figure 6. SEM images of functional cotton fabrics after (a) rubbing and (c) accelerated laundering; Enlarged partial SEM images of functional cotton fabrics after (b) rubbing and (d) accelerated laundering.

4. Conclusions

We herein reported our study into the microcapsule capsulating two substances (dye indigo and lavender essence) simultaneously, which was applied to cotton fabrics to obtain functional cotton fabrics. The adsorption behavior and adsorption mechanism for the DEMs onto cotton fabrics were studied by means of physicochemical properties and adsorption kinetics. Finally, the color fastness properties of functional cotton fabrics were investigated under practical application conditions. Results showed that DEMs were successfully prepared, with a mean particle size about 617 nm. In addition, lavender essence and indigo dye molecules were incorporated into DEMs. The combination of DEMs and cotton fabrics was facilitated by the formation of intramolecular hydrogen bonds. Furthermore, cotton fabrics could adsorb DEMs on the surface with three stages: fast adsorption, slow adsorption rate, and adsorption equilibrium. The cotton fabrics treated with DEMs had excellent color fastness performance. The residual DEMs was 81.4% and 21.7% after rubbing and intense accelerated laundering. Herein, we tried to deepen an understanding of the adsorption mechanism of microparticles on cotton fabrics surfaces. We therefore expect that this study will be beneficial to the development of functional cotton fabrics-based materials. In the current research, adsorption mechanism analysis for this system was limited to the kinetic mechanism, and the thermodynamic properties of the binding process (such as Langmuir isotherm adsorption model, Freundlich adsorption isotherm model and Dubinin–Radushkevich adsorption model, etc.) have not been studied yet. In the later research, the thermodynamic model will be further studied.

Supplementary Materials: The following are available online at <https://www.mdpi.com/article/10.3390/coatings11040426/s1>, Figure S1: the UV–Visible absorption spectrum of lavender essence and dye indigo, Figure S2: the standard curve of dye indigo solution, Table S1: the aroma compounds and their percentage in the lavender essence.

Author Contributions: Manuscript proofread: Q.K.; Study design: Q.K., Z.X., X.K. and Y.Z.; Data collection: W.X.; Writing: W.X.; Literature search: Z.X. and J.M.; Data analysis: Y.N.; Data analysis: X.K.; All authors have read and agreed to the published version of the manuscript.

Funding: This research was funded by Capacity building project of local universities Science and Technology Commission of Shanghai Municipality, grant number 19090503500; National Natural

Science Foundation of China, grant number 31901618; National Key Research and Development Program Nanotechnology Specific Project, grant number 2016YFA0200304 and China Postdoctoral Science Foundation, grant number 2020M681125.

Institutional Review Board Statement: Not applicable.

Informed Consent Statement: Not applicable.

Data Availability Statement: No applicable.

Conflicts of Interest: The authors declare no conflict of interest.

References

1. Shahid, M.; Mohammad, F. Recent advancements in natural dye applications: A review. *J. Clean. Prod.* **2013**, *53*, 310–331. [[CrossRef](#)]
2. Wang, S.; Zhang, W.; Chen, Y.; Zhang, S.; Wang, W. The Aromatic Properties of Polyurea-Encapsulated Lavender Oil Microcapsule and Their Application in Cotton Fabrics. *J. Nanosci. Nanotechnol.* **2019**, *19*, 4147–4153. [[CrossRef](#)] [[PubMed](#)]
3. Bagheri-Nesami, M.; Espahbodi, F.; Nikkhah, A.; Shorofi, S.A.; Charati, J.Y. The effects of lavender aromatherapy on pain following needle insertion into a fistula in hemodialysis patients. *Complementary Ther. Clin. Pract.* **2014**, *20*, 1–4. [[CrossRef](#)] [[PubMed](#)]
4. Ashrastaghi, O.; Ayasi, M.; Gorji, M.; Habibi, V.; Charati, J.; Ebrahimzadeh, M. The effectiveness of lavender essence on sternotomy related pain intensity after coronary artery bypass grafting. *Adv. Biomed. Res.* **2015**, *4*, 127. [[CrossRef](#)] [[PubMed](#)]
5. Davidov-Pardo, G.; Rocca, P.; Salgado, D.; Leon, A.E.; Pedroza-Islas, R. Utilization of Different Wall Materials to Microencapsulate Fish Oil Evaluation of its Behavior in Bread Products. *Am. J. Food Technol.* **2008**, *3*, 384–393. [[CrossRef](#)]
6. Davidov-Pardo, G.; Arozarena, I.; Marín-Arroyo, M.R. Optimization of a Wall Material Formulation to Microencapsulate a Grape Seed Extract Using a Mixture Design of Experiments. *Food Bioprocess Technol.* **2013**, *6*, 941–951. [[CrossRef](#)]
7. Gui-Xiang, H. Review of the microcapsule technology in the application of dyeing and finishing processes. *Text. Dye. Finish. J.* **2016**, 17–70. [[CrossRef](#)]
8. Li-Mei, Z.; Run-Ze, L.; Bing, L.; Zhu, T. The Progress of Micro-encapsulation Technology Applied in Dyeing and Finishing Industry. *Guangzhou Chem. Ind.* **2007**, *35*, 6–13.
9. Arfat, Y.A.; Ahmed, J.; Ejaz, M.; Mullah, M. Polylactide/graphene oxide nanosheets/clove essential oil composite films for potential food packaging applications. *Int. J. Biol. Macromol.* **2017**, *107*, 194–203. [[CrossRef](#)]
10. Sauraj, B.; Kumar, Y.S. Chitosan film incorporated with citric acid and glycerol as an active packaging material for extension of green chilli shelf life. *Carbohydr. Polym.* **2018**, *195*, 329–338.
11. Varona, S.; Rodríguez Rojo, S.; Martín, Á.; Cocero, M.J.; Serra, A.T.; Crespo, T.; Duarte, C.M.M. Antimicrobial activity of lavandin essential oil formulations against three pathogenic food-borne bacteria. *Ind. Crop. Prod.* **2013**, *42*, 243–250. [[CrossRef](#)]
12. Fetzner, A.; Böhm, S.; Schreder, S.; Schubert, R. Degradation of raw or film-incorporated β -cyclodextrin by enzymes and colonic bacteria. *Eur. J. Pharm. Biopharm. Off. J. Arb. Für Pharm. Verfahr. EV* **2004**, *58*, 91–97. [[CrossRef](#)]
13. Miranda, J.C.D.; Martins, T.E.A.; Veiga, F.; Ferraz, H.G. Cyclodextrins and ternary complexes: Technology to improve solubility of poorly soluble drugs. *Braz. J. Pharm. Sci.* **2011**, *47*, 665–681. [[CrossRef](#)]
14. Liu, K.; Ma, C.; Wu, T.; Qi, W.; Yan, Y.; Huang, J. Recent advances in assemblies of cyclodextrins and amphiphiles: Construction and regulation. *Curr. Opin. Colloid Interface Sci.* **2020**, *45*, 44–56. [[CrossRef](#)]
15. Zhou, C.C.; Cheng, X.H.; Yan, Y.; Wang, J.D.; Huang, J.B. Reversible Transition between SDS@2 β -CD Microtubes and Vesicles Triggered by Temperature. *Langmuir* **2014**, *30*, 3381–3386. [[CrossRef](#)] [[PubMed](#)]
16. Yan, Y.; Jiang, L.; Huang, J. Unveil the potential function of CD in surfactant systems. *Phys. Chem. Chem. Phys.* **2011**, *13*, 9074–9082. [[CrossRef](#)] [[PubMed](#)]
17. Jiang, L.; Peng, Y.; Yan, Y.; Huang, J. Aqueous self-assembly of SDS@2 β -CD complexes: Lamellae and vesicles. *Soft Matter* **2011**, *7*, 1726–1731. [[CrossRef](#)]
18. Jiang, L.; Peng, Y.; Yan, Y.; Deng, M.; Wang, Y.; Huang, J. “Annular Ring” microtubes formed by SDS@2 β -CD complexes in aqueous solution. *Soft Matter* **2010**, *6*, 1731–1736. [[CrossRef](#)]
19. Jiang, L.; Yan, Y.; Huang, J. Zwitterionic surfactant/cyclodextrin hydrogel: Microtubes and multiple responses. *Soft Matter* **2011**, *7*, 10417–10423. [[CrossRef](#)]
20. Zhou, C.; Cheng, X.; Zhao, Q.; Yan, Y.; Wang, J.; Huang, J. Self-Assembly of Nonionic Surfactant Tween 20@2 β -CD Inclusion Complexes in Dilute Solution. *Langmuir* **2013**, *29*, 13175–13182. [[CrossRef](#)]
21. Zhu, B.; Jia, L.; Guo, X.; Yin, J.; Zhao, Z.; Chen, N.; Chen, S.; Jia, Y. Controllable assembly of a novel cationic gemini surfactant containing a naphthalene and amide spacer with β -cyclodextrin. *Soft Matter* **2019**, *15*, 3198–3207. [[CrossRef](#)]
22. Guerrero-Martínez, A.; González-Gaitano, G.; Viñas, M.H.; Tardajos, G. Inclusion Complexes between β -Cyclodextrin and a Gemini Surfactant in Aqueous Solution: An NMR Study. *J. Phys. Chem. B* **2006**, *110*, 13819–13828. [[CrossRef](#)]
23. Jiang, L.; Deng, M.; Wang, Y.; Liang, D.; Yan, Y.; Huang, J. Special Effect of β -Cyclodextrin on the Aggregation Behavior of Mixed Cationic/Anionic Surfactant Systems. *J. Phys. Chem. B* **2009**, *113*, 7498–7504. [[CrossRef](#)]

24. Dai, C.; Yang, Z.; Yang, H.; Liu, Y.; Fang, J.; Chen, W.; Li, W.; Zhao, M. Micelle-to-vesicle transition induced by β -cyclodextrin in mixed cationic surfactant solutions. *Colloids Surf. A Physicochem. Eng. Asp.* **2016**, *498*, 1–6. [[CrossRef](#)]
25. Milcovich, G.; Antunes, F.E.; Grassi, M.; Asaro, F. Stabilization of unilamellar cationic vesicles induced by β -cyclodextrins: A strategy for a tunable drug delivery depot. *Int. J. Pharm.* **2018**, *548*, 474–479. [[CrossRef](#)]
26. Zacheo, A.; Bizzarro, L.; Blasi, L.; Piccirillo, C.; Cardone, A.; Gigli, G.; Ragusa, A.; Quarta, A. Lipid-Based Nanovesicles for Simultaneous Intracellular Delivery of Hydrophobic, Hydrophilic, and Amphiphilic Species. *Front. Bioeng. Biotechnol.* **2020**, *8*. [[CrossRef](#)] [[PubMed](#)]
27. Yuan, Y.; Zhang, Q.; Yan, Y.; Gong, M.; Zhao, Q.; Bao, Z.; Liu, K.; Wang, S. Designed construction of tween 60@ 2β -CD self-assembly vesicles as drug delivery carrier for cancer chemotherapy. *Drug Deliv.* **2018**, *25*, 623–631. [[CrossRef](#)] [[PubMed](#)]
28. Zheng, H.; Li, X.; Jia, Q. Design of pH-Responsive Polymer Monolith Based on Cyclodextrin Vesicle for Capture and Release of Myoglobin. *ACS Appl. Mater. Interfaces* **2018**, *10*, 5909–5917. [[CrossRef](#)]
29. Ma, J.; Xu, W.; Kou, X.; Niu, Y.; Xia, Y.; Wang, Y.; Tian, G.; Zhao, Y.; Ke, Q. Green Fabrication of Control-Released, Washable, and Nonadhesive Aromatic-Nanocapsules/Cotton Fabrics via Electrostatic-Adsorption/In Situ Immobilization. *ACS Sustain. Chem. Eng.* **2020**, *8*, 15258–15267. [[CrossRef](#)]
30. Rajendran, R.; Radhai, R.; Kotresh, T.M.; Csiszar, E. Development of antimicrobial cotton fabrics using herb loaded nanoparticles. *Carbohydr. Polym.* **2013**, *91*, 613–617. [[CrossRef](#)] [[PubMed](#)]
31. Liu, C.; Liang, B.; Wang, Y.; Li, Y.; Shi, G. Core-shell nanocapsules containing essential oil for textile application. *J. Appl. Polym. Sci.* **2018**, *135*, 45695. [[CrossRef](#)]
32. Hansson, S.; Tischer, T.; Goldmann, A.S.; Carlmark, A.; Barner-Kowollik, C.; Malmström, E. Visualization of poly (methyl methacrylate) (PMMA) grafts on cellulose via high-resolution FT-IR microscopy imaging. *Polym. Chem.* **2012**, *3*, 307–309. [[CrossRef](#)]
33. Ma, L.; Zhao, D.; Zheng, J. Construction of electrostatic and π - π interaction to enhance interfacial adhesion between carbon nanoparticles and polymer matrix. *J. Appl. Polym. Sci.* **2020**, *137*, 48633. [[CrossRef](#)]
34. Xiao, Z.; Jia, J.; Niu, Y.; Zhu, G.; Kou, X. The adsorption mechanism of poly-methyl methacrylate microparticles onto paper cellulose fiber surfaces without crosslinking agents. *J. Appl. Polym. Sci.* **2020**, *137*, 49269. [[CrossRef](#)]
35. Rungwasantisuk, A.; Raibhu, S. Application of encapsulating lavender essential oil in gelatin/gum-arabic complex coacervate and varnish screen-printing in making fragrant gift-wrapping paper. *Prog. Org. Coat.* **2020**, *149*, 105924. [[CrossRef](#)]
36. Siva, S.; Li, C.; Cui, H.; Meenatchi, V.; Lin, L. Encapsulation of essential oil components with methyl- β -cyclodextrin using ultrasonication: Solubility, characterization, DPPH and antibacterial assay. *Ultrason. Sonochem.* **2020**, *64*, 104997. [[CrossRef](#)]
37. Fizer, M.M.; Mariychuk, R.T.; Fizer, O.I. Gold nanoparticles green synthesis with clove oil: Spectroscopic and theoretical study. *Appl. Nanosci.* **2021**, 1–10. [[CrossRef](#)]
38. Ju, Z.; Sun, J.; Liu, Y. Molecular Structures and Spectral Properties of Natural Indigo and Indirubin: Experimental and DFT Studies. *Molecules* **2019**, *24*, 3831. [[CrossRef](#)] [[PubMed](#)]
39. Xiao, Z.; Liu, W.; Zhu, G.; Zhou, R.; Niu, Y. Production and characterization of multinuclear microcapsules encapsulating lavender oil by complex coacervation. *Flavour Fragr. J.* **2014**, *29*, 166–172. [[CrossRef](#)]
40. Baran, A.; Fiedler, A.; Schulz, H.; Baranska, M. In situ Raman and IR spectroscopic analysis of indigo dye. *Anal. Methods* **2010**, *2*, 1372–1376. [[CrossRef](#)]
41. Platania, E.; Lofrumento, C.; Lottini, E.; Azzaro, E.; Ricci, M.; Becucci, M. Tailored micro-extraction method for Raman/SERS detection of indigoids in ancient textiles. *Anal. Bioanal. Chem.* **2015**, *407*, 6505–6514. [[CrossRef](#)]
42. Wang, M.; She, Y.; Xiao, Z.; Hu, J.; Zhou, R.; Zhang, J. The green adsorption of chitosan triphosphate nanoparticles on cotton fiber surfaces. *Carbohydr. Polym.* **2014**, *101*, 812–818. [[CrossRef](#)] [[PubMed](#)]
43. Xiao, Z.; Hou, W.; Kang, Y.; Niu, Y.; Kou, X. Encapsulation and sustained release properties of watermelon flavor and its characteristic aroma compounds from γ -cyclodextrin inclusion complexes. *Food Hydrocoll.* **2019**, *97*, 105202. [[CrossRef](#)]
44. Yang, Z.; Yao, X.; Xiao, Z.; Chen, H.; Ji, H. Preparation and release behaviour of the inclusion complexes of phenylethanol with β -cyclodextrin. *Flavour Fragr. J.* **2016**, *31*, 206–216. [[CrossRef](#)]
45. Xiao, Z.; Kang, Y.; Hou, W.; Niu, Y.; Kou, X. Microcapsules based on octenyl succinic anhydride (OSA)-modified starch and maltodextrins changing the composition and release property of rose essential oil. *Int. J. Biol. Macromol.* **2019**, *137*, 132–138. [[CrossRef](#)] [[PubMed](#)]
46. Xiao, Z.; Xu, J.; Niu, Y.; Zhu, G.; Kou, X. Effects of Surface Functional Groups on the Adhesion of SiO₂ Nanospheres to Bio-Based Materials. *Nanomaterials* **2019**, *9*, 1411. [[CrossRef](#)] [[PubMed](#)]
47. Ding, L.; Deng, H.; Wu, C.; Han, X. Affecting factors, equilibrium, kinetics and thermodynamics of bromide removal from aqueous solutions by MIEEX resin. *Chem. Eng. J.* **2012**, *181–182*, 360–370. [[CrossRef](#)]
48. Liu, Y.; Ying, D.; Sanguansri, L.; Augustin, M.A. Comparison of the adsorption behaviour of catechin onto cellulose and pectin. *Food Chem.* **2019**, *271*, 733–738. [[CrossRef](#)]
49. Pignatello, J.J.; Xing, B. Mechanisms of Slow Sorption of Organic Chemicals to Natural Particles. *Environ. Sci. Technol.* **1996**, *30*, 1–11. [[CrossRef](#)]
50. Hatton, F.L.; Malmström, E.; Carlmark, A. Tailor-made copolymers for the adsorption to cellulosic surfaces. *Eur. Polym. J.* **2015**, *65*, 325–339. [[CrossRef](#)]

51. Wang, M.; Fu, H.; She, Y.; Xiao, Z.; Zhu, G.; Hu, J. Adsorption capacity, kinetics, and thermodynamics of chitosan nanoparticles onto cotton fabrics without any chemical binders. *Polym. Compos.* **2015**, *36*, 2093–2102. [[CrossRef](#)]
52. Gopakumar, D.A.; Pasquini, D.; Henrique, M.A.; de Moraes, L.C.; Grohens, Y.; Thomas, S. Meldrum's Acid Modified Cellulose Nanofiber-Based Polyvinylidene Fluoride Microfiltration Membrane for Dye Water Treatment and Nanoparticle Removal. *ACS Sustain. Chem. Eng.* **2017**, *5*, 2026–2033. [[CrossRef](#)]
53. Zambrano-Intriago, L.A.; Gorozabel-Mendoza, M.L.; Córdova Mosquera, A.; Delgado-Demera, M.H.; Duarte, M.M.M.B.; Rodríguez-Díaz, J.M. Kinetics, equilibrium, and thermodynamics of the blue 19 dye adsorption process using residual biomass attained from rice cultivation. *Biomass Convers. Biorefin.* **2020**, 11–13. [[CrossRef](#)]
54. Grabi, H.; Lemlikchi, W.; Derridj, F.; Lemlikchi, S.; Trari, M. Efficient native biosorbent derived from agricultural waste precursor for anionic dye adsorption in synthetic wastewater. *Biomass Convers. Biorefin.* **2021**, 1–18. [[CrossRef](#)]
55. Taleb, K.; Markovski, J.; Veličković, Z.; Rusmirović, J.; Rančić, M.; Pavlović, V.; Marinković, A. Arsenic removal by magnetite-loaded amino modified nano/microcellulose adsorbents: Effect of functionalization and media size. *Arab. J. Chem.* **2019**, *12*, 4675–4693. [[CrossRef](#)]
56. Naseri, K.; Allahverdi, A. Methylene blue adsorption by TiO₂-based nano-adsorbents: Performance evaluation and kinetic study. *Res. Chem. Intermed.* **2019**, *45*, 4863–4883. [[CrossRef](#)]
57. Wang, H.; Xie, R.; Zhang, J.; Zhao, J. Preparation and characterization of distillers' grain based activated carbon as low cost methylene blue adsorbent: Mass transfer and equilibrium modeling. *Adv. Powder Technol.* **2018**, *29*, 27–35. [[CrossRef](#)]
58. Prajapati, A.K.; Mondal, M.K. Comprehensive kinetic and mass transfer modeling for methylene blue dye adsorption onto CuO nanoparticles loaded on nanoporous activated carbon prepared from waste coconut shell. *J. Mol. Liq.* **2020**, *307*, 112949. [[CrossRef](#)]